Ultrasound in Med. & Biol., Vol. ■, No. ■, pp. 1–9, 2009

0301-5629/09/$–see front matter

ELSEVIER

doi:10.1016/j.ultrasmedbio.2009.05.020

● *Original Contribution*

ULTRAFAST IMAGING OF ULTRASOUND CONTRAST AGENTS

Olivier Couture,*† Souad Bannouf,* Gabriel Montaldo,* Jean-François Aubry,* Mathias Fink,* and Mickael Tanter*‡

*Institut Langevin Ondes et Images (CNRS UMR 7587), École Supérieure de Physique et de Chimie Industrielle, Paris, France; †Fondation Pierre-Gilles de Gennes, Paris, France; and ‡INSERM, Paris, France

(*Received* 31 *December* 2008, *revised* 14 *May* 2009, *in final form* 25 *May* 2009)

Abstract—The disappearance of ultrasound contrast agents after disruption can provide useful information on their environment. However, *in vivo* acoustical imaging of this transient phenomenon, which has a duration on the order of milliseconds, requires high frame rates that are unattainable by conventional ultrasound scanners. In this article, ultrafast imaging is applied to microbubble tracking using a 128-element linear array and an elastography scanner. Contrast agents flowing in a wall-less tissue phantom are insonified with a high-intensity disruption pulse followed by a series of plane waves emitted at a 5 kHz PRF. A collection of compounded images depicting the evolution of microbubbles is obtained after the echoes are beamformed *in silico*. The backscattering of the microbubbles appears to increase in the first image after disruption (4 ms) and decrease following an exponential decay in the next hundred milliseconds. This microbubble dynamic depends on the length and amplitude of the high-intensity pulse. Furthermore, confined microbubbles are found to differ significantly from their free-flowing counterparts in their dissolution curves. The high temporal resolution provided by ultrafast imaging could help distinguish targeted microbubbles during molecular imaging. (E-mail:olicou@gmail.com) © 2009 World Federation for Ultrasound in Medicine & Biology.

Key Words: **Microbubbles, Disruption, Plane waves, Dissolution, Ultrafast, Targeted contrast agents, Molecular imaging.**

INTRODUCTION

Micron-sized encapsulated bubbles are currently used as blood-pool contrast agents for ultrasound imaging. Microbubble detection relies on their nonlinear acoustic behaviour, which is highlighted by pulse sequences such as harmonic filtering, pulse-inversion, amplitude modulation or radial modulation (de Jong et al. 2000; Simpson et al. 1999; Eckersley et al. 2005; Masoy et al. 2008). Microbubbles can also be disrupted by pulses at acoustic pressures that do not affect tissue (Porter and Xie 1995). Therefore, comparing frames before and after disruption yields very high contrast-to-tissue ratios (CTR). The rate at which new microbubbles repopulate a plane after disruption can also provide information on tissue perfusion. For instance, cardiac ischemia and angiogenic tumours can be assessed with disruption-reperfusion imaging (Wei et al. 1998; Wilson and Burns 2006).

High-speed optical observations of single microbubble have shown that their disruption occurs when acoustic pressures reach a threshold, which varies with frequency and the strength of the protective shell (Bouakaz et al. 2005; Postema et al. 2005a, 2005b). The violent oscillations cause the membrane of the contrast agent to crack and the gas to be released as a free bubble. The gas then dissolves at a rate that depends on its diffusion rate (normally that of air or perfluorocarbon), on the bubble radius and on the hydrostatic pressure of the environment (Bouakaz et al. 1999). The dissolution time is typically in the range of 10 to 100 ms for commercial contrast agents (Bouakaz et al. 2007). However, this process can be accelerated by the fragmentation of the microbubbles into smaller particles (Chomas et al. 2001; Bevan et al. 2008).

In addition to optical observations, the dissolution of microbubbles postdisruption has been studied with single-element ultrasound transducers (Bevan et al. 2007; Chen et al. 2002). These experiments were done by performing pulse-echo along a single ultrasonic line at a high repetition rate (few kHz) in chambers containing low concentrations of microbubbles. An enhancement in backscattering was often observed just after disruption. This phenomenon was explained either by the decrease in membrane damping after disruption or by a passage of the bubble

Address correspondence to: Olivier Couture, Ph.D., Laboratoire Ondes et Acoustique École Supérieure de Physique et Chime Industrielle, 10 rue Vauquelin, Paris, 75005, France. E-mail: olicou@gmail.com

through the resonant size during dissolution. In the simplest cases, the signal decline of the microbubbles could be fitted to an exponential decay.

Since the dissolution of microbubbles depends on their environment, the evolution of their acoustic scattering after disruption contains relevant physiologic information. For example, Bouakaz et al. (1999) proposed to measure arterial pressure noninvasively by exploiting microbubble disruption. Moreover, we can postulate that the disruption of targeted microbubbles or those confined in microvessels might differ from free-flowing ones due to asymmetrical tensions in their membrane (Caskey et al. 2007; Garbin et al. 2007; Zhao et al. 2005). Such differentiation can become a useful tool for ultrasound molecular imaging (Dayton and Rychak 2007). Unfortunately, measuring the rapid process of the dissolution of moving bubbles requires the ultrasonic imaging of an entire plane at frame rates in the kHz range, which is unattainable with current ultrasound scanners. Indeed, because B-mode imaging is performed by successively focusing a beam on each line, commercial scanners acquire at a maximum frame rate of about 60 Hz. Using such a conventional approach, dissolution imaging could be performed line by line, but it would require as many disruption events as the number of lines. Moreover, since disruption cannot be limited to a single line, complete reperfusion of the microbubbles through tissue would be required between each acquisition. Pauses of several seconds would lead to impractical imaging times and motion artefacts that affect dissolution-based contrast. The development of an ultrafast dissolution imaging sequence as presented in this article solves this problem.

The concept of ultrafast imaging was introduced by Shattuck and coworkers (1984). Although the so-called Explososcan consisted in four parallel receive beamformers, they envisioned extending this technique to perform one echographic image per ultrasonic emission, allowing kHz frame rates. Such an ultrafast system was introduced by our laboratory in the context of transient elastography (Sandrin et al. 2002). Ultrafast tracking of shear waves induced by radiation force was developed to assess tissue elasticity (Sarvazyan et al. 1998; Bercoff et al. 2002, 2004; Tanter et al. 2002). Applications in breast cancer diagnosis (Tanter el al. 2008), musculoskeletal system elasticity estimation (Deffieux et al. 2006) and liver fibrosis staging (Muller et al. 2008) are promising.

The ultrafast frame rate is achieved by emitting plane waves with an ultrasound array, collecting the echoes from tissues and backpropagating them *a posteriori in silico*. Within the time a single line is acquired in conventional imaging, a full image can be obtained with the ultrafast method receive parallel beamforming leading to frame rates over 7000 Hz. However, since the ultrasound beams are not focused in the transmit mode, signal-to-noise ratio (SNR) and contrast are reduced. Recently, Montaldo et al. (2009) demonstrated that SNR and contrast can be regained by combining coherently backscattered echoes from successive compounded plane wave insonifications at different angles. For most applications, less than seven compounded angles are sufficient, reducing the frame rate to 1000 Hz, which would be adequate to assess microbubbles evolution (Montaldo et al. 2009). A plane wave imaging technique would make the observation of the dissolution process of microbubbles *in vivo* practical technically and allow the exploitation of new contrast mechanisms.

In this study, we present a method for the ultrafast B-mode imaging of the transient dissolution of microbubbles just after their disruption. Images of microbubbles within a wall-less vessel phantom are analysed to assess their rapid evolution for different disruption pulses. Several bubble detection methods are applied to ultrafast imaging, including a new representation of the spatial distribution of their disruption dynamics. Finally, the dissolution of microbubbles in solution is briefly compared with that of bound agents.

MATERIAL AND METHODS

Device and ultrafast disruption imaging sequence

Ultrafast imaging can be implemented on fully programmable ultrasound scanners relying on sufficient data transfer rates and memory capabilities. For this study, an ultrafast two-dimensional (2-D) elastography scanner (V1; Supersonic Imagine, Aix-En-Provence, France) with 2 GB/s data transfer rate was adapted to disrupt microbubbles. The scanner was equipped with an 8 MHz linear array (Vermon, Tours, France). The first step of the technique consisted in sending a series of plane waves (8 MHz, 2 cycles, 184 kPa) and accumulating the echoes in memory (Fig. 1a). In this first imaging phase, 55 plane waves were emitted with different pulse repetition frequencies (2750 Hz or 5500 Hz). Eleven plane waves with –10 to 10 degrees tilts were used to form an image, so that five compounded images were obtained after coherent synthetic recombination (frame rate: 250 Hz or 500 Hz). In the second phase, the disruption pulse was emitted, which was a 5 MHz plane wave with varying pressures (from 100 to 440 kPa peak negative pressure at 2.5 cm depth) and pulse lengths (from 10 to 20,000 us). After disruption, the imaging process was repeated, this time with 65 B-mode images formed with 715 plane waves. This ultrafast-dissolution (UD) pulse sequence lasted 140 ms, which was sufficient to follow the whole disruption process. After the echoes were recorded and saved in the emission-reception board, they were transferred all at once to the beamforming computer, allowing very high-frame rates during short bursts of time.

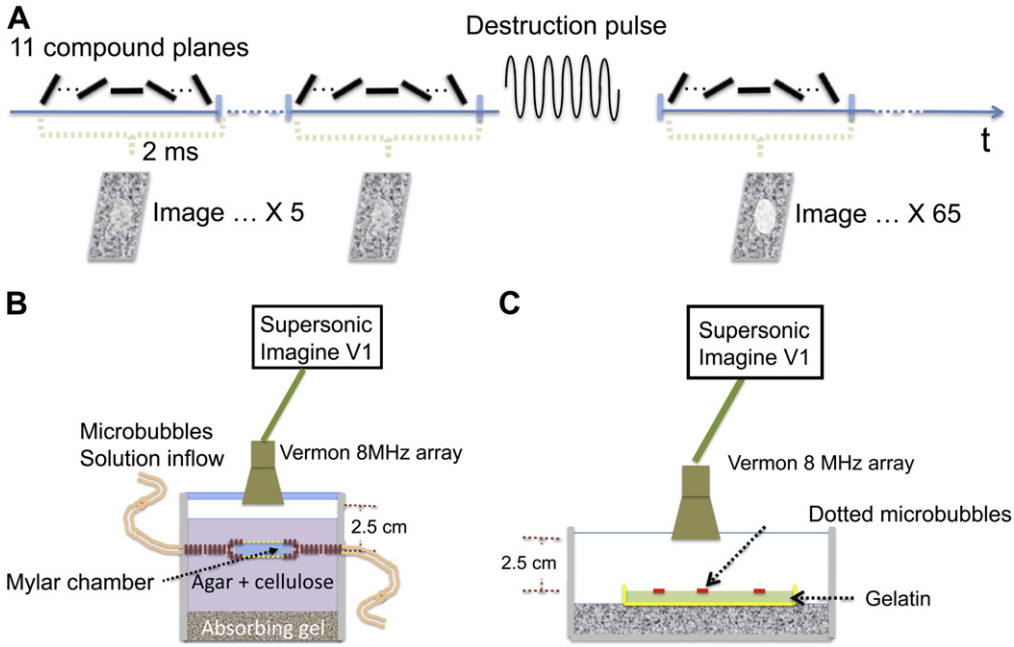

Fig. 1. Set-up for the ultrafast imaging of microbubbles within a vessel. (a) Pulse sequence for ultrafast acquisition of disruption. Five compounded images are acquired prior to disruption and 65 B-mode images are acquired afterward. (b) Microbubbles in solution: The chamber is either wall-less or reinforced with a Mylar membrane. The linear array is placed perpendicularly to the direction of the flow. (c) Bound microbubbles: The linear array is placed 2.5 cm away from the surface of gelatin where microbubbles were deposited.

Data accumulated in the acquisition card were transferred to a computer for analysis by Matlab (Mathworks, Natick, MA, USA). Raw RF images were obtained by coherent recombination of the backscattered echoes from successive plane waves illuminations to perform a synthetic transmit beam and then beamforming the data in the receive mode (Montaldo et al. 2009). The backscattered intensity of the microbubbles was obtained by averaging the power in the regions-of-interest, either in the vessel or in the tissue phantom. Additionally, by subtracting images obtained before disruption and 30 ms later, conventional disruption imaging could be reproduced with plane waves.

Ultrafast nonlinear pulse inversion and amplitude modulation sequences

In parallel to dissolution imaging of microbubbles, classic nonlinear pulse sequences such as pulse-inversion and amplitude modulation were also executed in the context of ultrafast imaging. For instance, rather than applying the pulse-inversion scheme over each line, the scheme was implemented with plane waves so that the entire field of view was insonified with pulses of alternating phase. Plane wave imaging was implemented using unfocused pulses with opposite phases and different steering angles separated by less than 0.4 ms. The frames obtained from the synthetic beamforming of the compounded echoes were summed to form plane-wave pulse-inversion (PWPI) images. Additionally, images were also formed with plane waves emitted alternatively by the odd elements, the even elements and the entire array. Such a pulse-sequence is referred as plane-wave amplitude modulation (PWAM).

Experimental set-up

Dissolution imaging was performed on microbubbles in a solution and bound microbubbles. A wall-less vessel phantom was prepared by creating a tunnel, 5 mm in diameter, through a tissue phantom (Fig. 1b). For the dissolution experiment (Figs. 2 to 5), a Mylar membrane (Rescue Blanket 13 μm thick; Distrimed, France) was wrapped on the outside of the vessel to increase its strength. Lipid-shelled ultrasound contrast agents (Bracco Research, Switzerland), were diluted down to a 1/10,000 v/v concentration (about 120,000 microbubbles/mL) in degassed water. The solution was then made to flow by gravity through the wall-less vessel phantom. To isolate the effect of microbubble dissolution from replenishment due to motion, flow was stopped 15 s before the different imaging sequences (plane-wave fundamental imaging, PWPI, PWAM, plane-wave disruption, UD) were initiated.

Bound microbubble preparation

The bound microbubbles were prepared as described by Couture et al. (2009). Briefly, a 15 μL droplet of diluted avidinated microbubbles (2% v/v) was deposited on

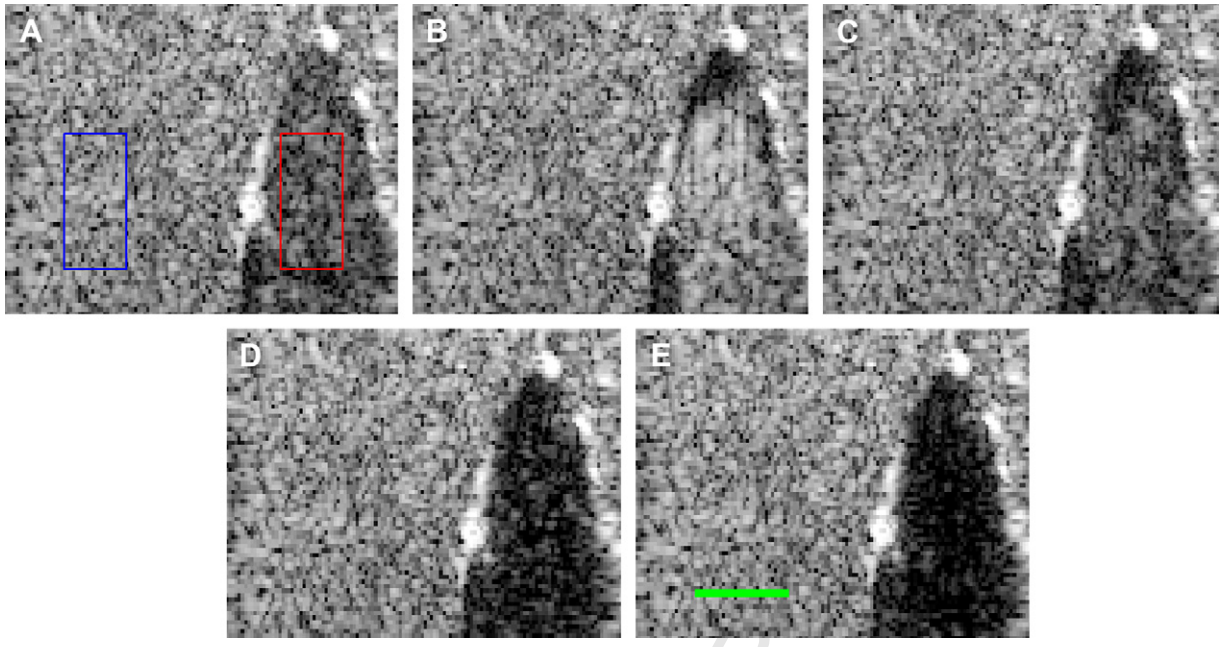

Fig. 2. Disruption of microbubbles in a wall-less vessel phantom imaged at 250 Hz. Time after disruption pulse shown. (a) The left square circumscribe the region where the tissue phantom signal is averaged. The right square delimitates the bubble signal. The bar (e) is 1 cm long. The grey-scale level ranges from –50 dB to –10 dB.

a gelatin surface (5% w/v) doped with biotin (1% w/v). After waiting 15 min, the surface was washed three times with PBS, leaving a disk of bound microbubbles 5 mm in diameter. The gel was then immersed in degassed PBS and placed 2.5 cm below the 8 MHz linear array. The same imaging sequence performed on the microbubbles in solution was executed on the bound microbubbles.

RESULTS

Figure 2 shows selected images of the dissolution of microbubbles within a wall-less vessel. In this fundamental mode, the microbubble solution in the predisruption stage appeared hypoechoic with respect to the tissue phantom. The border of the vessel was clearly delineated. In the first image after disruption (4 ms), most of the vessel's cross-section became brighter. In the centre of the vessel, the average backscatter intensity increased by 10 dB. However, a small region at the top of the vessel exhibited a decrease in microbubble signal by about 10 dB. In ultrafast images, the hyperechogenicity observed

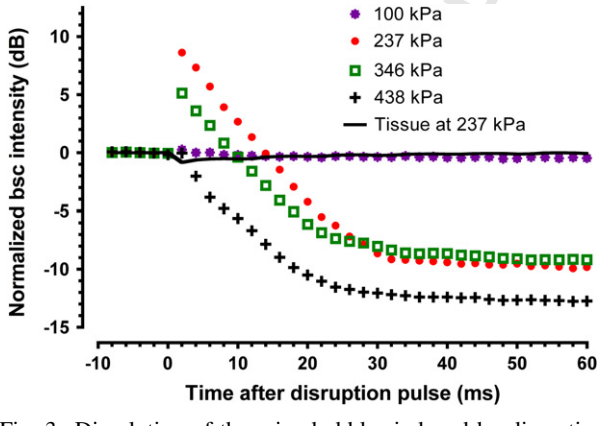

Fig. 3. Dissolution of the microbubbles induced by disruption pulses at different peak-pressure (fixed pulse length at 300 us). The backscattering (bsc) intensity is an average over a cross-section of the vessel. The time origin corresponds to the disruption pulse.

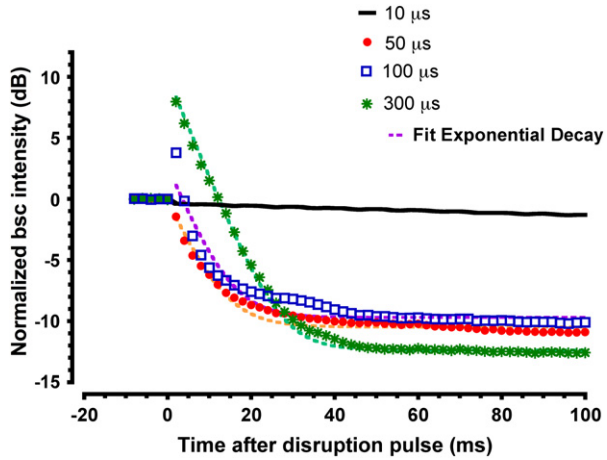

Fig. 4. Dissolution of the microbubbles induced by disruption pulses with various pulse-length (fixed pressure at 240 kPa). Exponential fit (equation: $I = I_0 e^{-Kt} + I_C$) of the backscattering intensity after disruption. The time-constant (K) is 0.177 ± 0.006 ms^{-1} for the 50 μs disruption pulse ($R^2 = 0.98$) and 0.192 ± 0.001 ms^{-1} for the 300 μs disruption pulse ($R^2 = 0.999$).

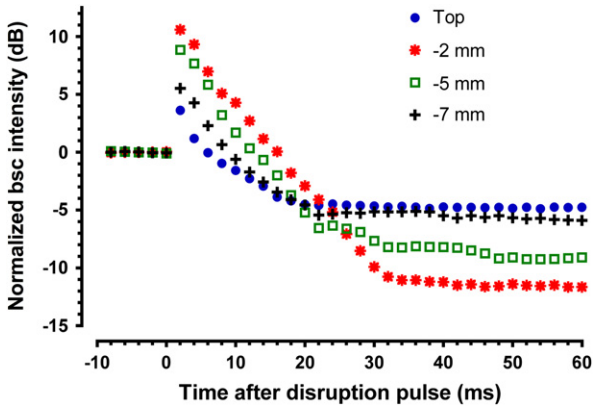

Fig. 5. Dissolution of the microbubbles for various depths thanks to backscatter intensity averaging over time windows. Disruption is induced by pulses at 237 kPa and 300 μs long.

in the early phase decayed slowly to disappear almost completely at 100 ms. At that point, the whole vessel was less echoic than prior to disruption.

Figure 3 shows the evolution of the backscattering intensity in the centre of the vessel for different disruption pulses at various pressures. The values are normalized with respect to the average of the first five predisruption images. As a control, the change in tissue signal is also shown, which shows a slight decrease in scattering intensity at time 0 before returning gradually to original levels in the next 50 ms. This overall drop in the signal that follow the disruption pulse is due to the transient response in the main power supply of the pulse generators. For disruption pulses at low pressures, the backscattering intensity of microbubbles is unchanged by the pulsing scheme. When disruption pressures are higher, backscatter intensity increases but then rapidly decays, losing 20 dB in 30 ms before reaching a plateau. For disruption pressures at 438 kPa, microbubble scattering did not increase after disruption but decayed rapidly to even lower levels. The speed of decay was found to be quite similar for different disruption pressures. The pulse-length dependence of the disruption process is shown in Figure 4. Short plane pulses (10 μs long) did not affect the microbubbles. However, a linear loss of backscattered intensity, down to –1.5 dB, was observed over the whole imaging sequence. Longer pulse (50 μs) disrupted the microbubbles leading to a loss in signal of about 10 dB. When disruption pulses longer than 100 μs were used, a peak enhancement in intensity was observed just after disruption. This enhancement lasted up to 25 ms, for maximum increase up to 8 dB. Here, the speed of the decay was found to be strongly dependent of the disruption pulse duration. The loss of signal after disruption followed an exponential decay curve (coefficient of correlation, $R^2 > 0.98$). The time-constant describing this exponential decay curve varied slightly between microbubbles dissolving from a peak enhancement and those that collapsed from their predisruption scattering level.

The spatial heterogeneity of the microbubble dissolution is shown in Figure 5. At the top of the vessel, the scattering from microbubbles was increased slightly postdisruption. The normalized signal then collapsed to –5dB at the end of the dissolution process. However, 2 mm under this region, the microbubbles were more affected. Scattering increased by 10 dB before collapsing to a minimum level of –13 dB. As the depth increased, the effect of disruption became less obvious.

Figure 6 shows a series of examples for ultrafast imaging exploiting varying techniques of contrast enhancement. All these images were created with plane wave emissions; where necessary pulse inversion or amplitude modulation sequences were interlaced between the compounding angles. The time between the acquisition of frames with opposite phase was less than 0.4 ms. For fair comparison, the same color bar was used in all images. When water was filling the tube and imaging was performed in fundamental mode (Fig. 6a), the wall-less vessel could be distinguished from surrounding tissue phantom. However, some contaminating signal could be observed at –14 dB. When microbubbles were added to the solution, the border disappeared and the scattering intensity for both regions became equivalent (Fig. 6b). Microbubbles were apparent when the sum of the echoes of pulses with opposite phase was used to produce the image (Fig. 6c, PWPI). This pulse-inversion imaging increased contrast-to-tissue ratio to 15 dB. Ultrafast amplitude modulation (Fig. 6d, PWAM) was also performed by alternatively emitting the pulses with the odd, even and all the elements. Contrast-to-tissue ratio was 21 dB and tissue phantom appeared more uniform when compared to pulse-inversion.

Disruption of the microbubbles increased CTR by 30 dB. Figure 6e shows the subtraction of the scattering intensity before disruption and at the end of dissolution as is common in disruption-reperfusion imaging. Thanks to the ultrafast mode, a new representation of the dissolution of microbubbles was introduced. The loss of signal during the first 4 ms after the disruption pulse is shown in Figure 6f. The slope of the decay in intensity is measured at every point and the positive and negative values are normalized and colour-coded independently. Green represents the region where the scattering increased after the disruption pulse and red represents the region of rapid decrease. The process of dissolution varied with respect to position within the wall-less vessel phantom. The microbubbles on top of the vessel did not demonstrate a postdisruption peak in enhancement as in the centre of the vessel.

Dissolution imaging was also attempted on microbubbles bound on a gelatin surface. Figure 7 shows the evolution of the reflection of the dot of microbubbles

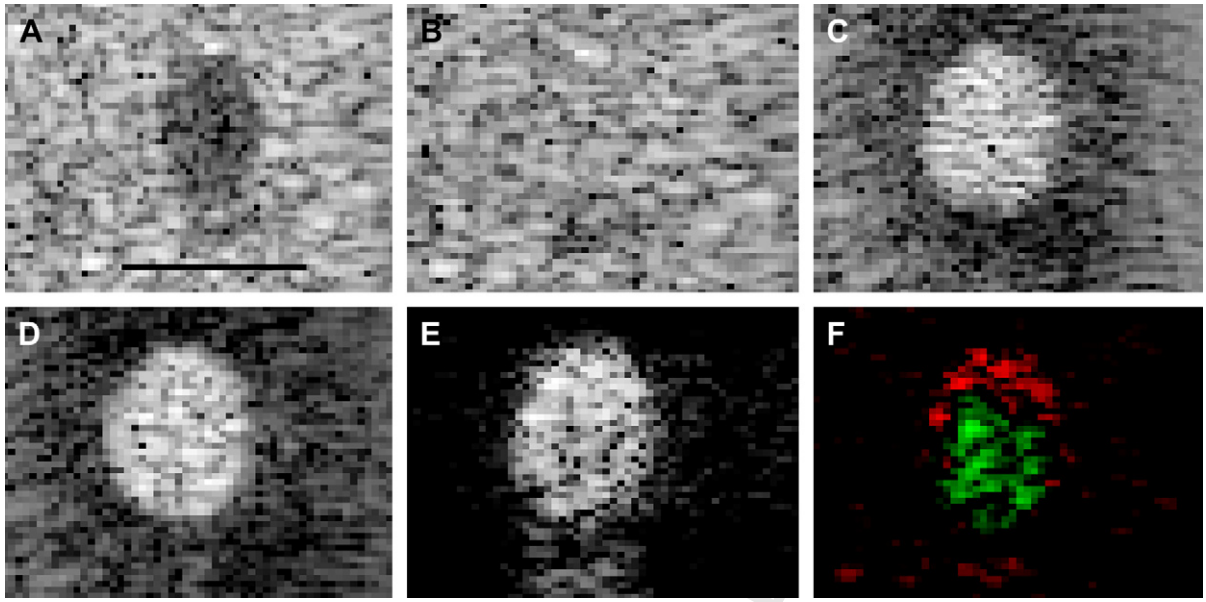

Fig. 6. Ultrafast imaging with various pulse sequences of a wall-less vessel filled with microbubbles. (a) Plane waves fundamental, no bubbles. (b) Fundamental. (c) Plane-waves pulse-inversion. (d) Plane waves amplitude-modulation. (e) Slow disruption. (f) Contrast based on the rate of change of the scattering within the first 4 ms after the disruption pulse. The scale bar is 1 cm long.

100 ms postdisruption pulse. Before disruption, the microbubbles appeared as a 3 mm-wide bright spot on the surface of gelatin. Postdisruption, the scattered intensity dropped and remained at such level until the end of the imaging time. The contrast from the microbubbles did not completely disappear after disruption. This experiment was repeated on six dots of microbubbles and the evolution of the backscattered intensity of bound microbubbles is compared with microbubbles in solution in Figure 8. For the same pulse-sequence, bound microbubbles did not show a postdisruption enhancement peak but instead a quick drop to –15 dB.

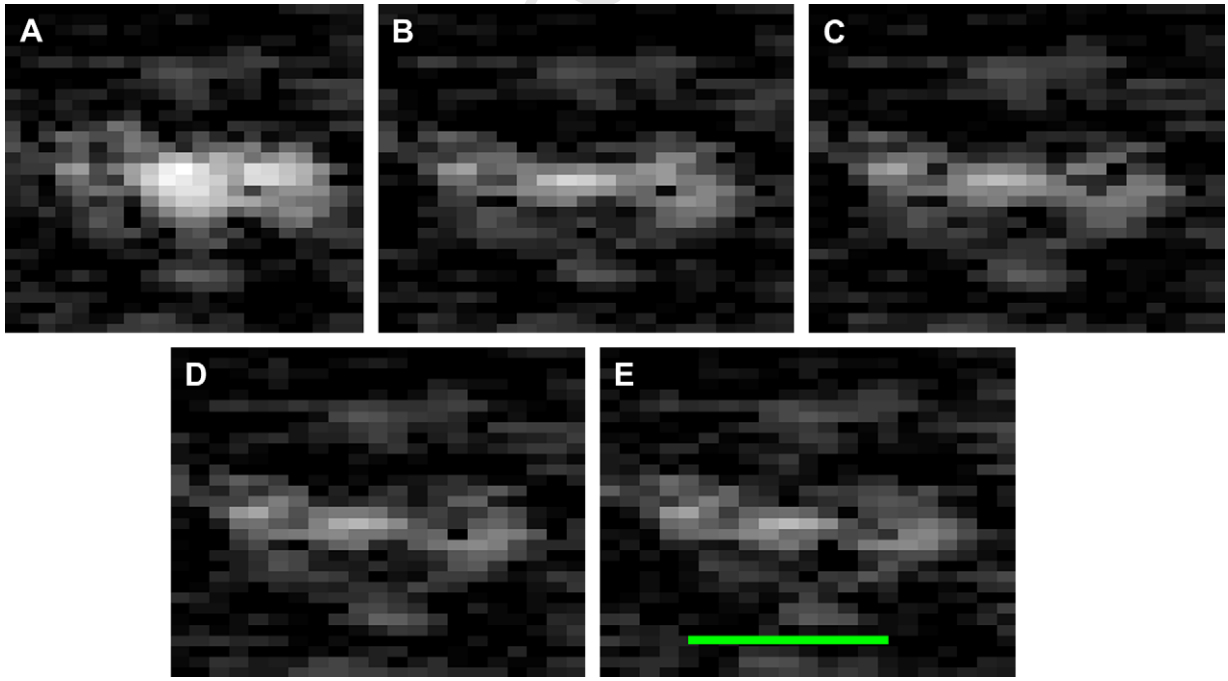

Fig. 7. Disruption of a microbubble dot on a surface of gelatin imaged at 250 Hz. Time after disruption pulse shown. The bar (e) is 3 mm long.

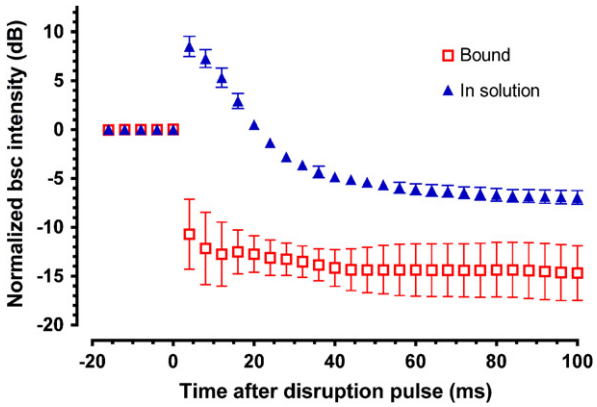

Fig. 8. Difference in the dissolution of bound and free-flowing microbubbles. The scattering of the bound microbubbles is averaged over the region of the dot on the surface of the gelatine (number of repetitions, $n = 6$), while the scattering of the bubbles in solution is averaged over a window inside the vessel ($n = 6$).

DISCUSSION

The dissolution of microbubbles postdisruption has already been studied with single-element ultrasound transducers (Bevan et al. 2007; Chen et al. 2002). Since the dissolution of microbubbles depends on their environment, the rapid evolution of their scattering properties contains relevant physiologic information. Nevertheless, in clinical situations, conventional echo has insufficient frame rate to track dissolving and moving microbubbles.

In this study, ultrafast B-mode with 500 Hz frame rate has allowed us to image the rapid dissolution of ultrasound contrast agent. In ultrafast imaging, there is a trade-off between signal-to-noise ratio and frame rate. Since ultrasound beams are not focused, lower pressures are attained at each observation point, leading to a lower signal. Pulse pressure is also reduced gradually with depth by attenuation. However, SNR is regained by increasing the number of plane waves emitted at different angles. The missing transmit focusing is replaced by a coherent recombination of the successive backscattered echoes. In such a set-up, microbubbles are insonified several times with lower amplitude pulses, spatially spread over the entire imaged area, rather than only one single time with higher amplitude at focus. Since the new generation of microbubbles is more sensitive (de Jong et al. 2007), they appear to remain nonlinear even when insonified with plane waves.

Plane wave compounding is exploited for the series of images shown in Figure 2. Despite the very high frame rate (250 Hz), the borders of the vessel are still clearly defined. The solution of microbubbles is also easily distinguished from surrounding tissue. Therefore, movies showing every step of the microbubbles dissolution can give a qualitative appreciation of very these high speed processes. For instance, a peak in enhancement after disruption is observable. Such an effect was observed in single-element experiments, but is difficult to exploit on regular scanners. Effectively, at a 30 Hz frame rate, only predisruption and steady-state (after 30 ms) acoustic behaviour can be observed. A difference in microbubble dissolution is also seen over the cross-section of the vessel, showing that rapid B-mode imaging might provide new information on the geometry and the local environment of bubble clouds.

Movies of dissolution of ultrasound contrast agents can also yield quantitative assessment on the evolution of a population of microbubbles after disruption. In Figures 3 and 4, the agents' behaviour is modified by changes in the disruption pulse. For instance, in Figure 3, low amplitude disruption pulses are seen to have little effect on the microbubbles. Very high amplitude pulses induce a fast exponential decay of the backscattered intensity. For medium amplitudes, a peak enhancement is observed before decay. Such behaviour seems to confirm that, for emission amplitudes higher than the disruption threshold, microbubble gas is freed from its shell and left to dissolve. This also confirms, on 2D images, results that were obtained in single-transducer experiments where the microbubbles released from their shell were capable of oscillating more violently, yielding higher scattering fractions (Bevan 2007). However, in this study, such an effect is difficult to distinguish from the transition of the dissolving microbubbles through their resonant size.

The absence of peak enhancement at higher pressure could mean that the microbubbles are fragmented in smaller gas pockets, leading to faster dissolution and lower scattering (Chomas et al. 2001; Bevan et al. 2008). Because the disruption threshold and the fragmentation threshold are dependent on both the pulse-length and the pressure, peak enhancement is only observed over a limited range of these parameters.

In the presence of peak enhancement, the decrease in the scattering intensity of microbubbles fits well with an exponential decay. Again, such a result corresponds to observations with single-transducers (Bevan et al. 2008). The scattering half-life seen on the 2D images is around 4 ms, which demonstrates the importance of ultrafast imaging to resolve the dissolution in the time domain. Accepting lower SNR, the frame rate of ultrafast could be increased up to 5000 Hz by reducing the number of compounding angles.

In this study, fairly long disruption pulses are used (300 us) to optimize the postdisruption peak enhancement. Short disruption pulses are not sufficient to disrupt the bubbles because only low pressures are attained with plane waves (438 kPa). It is easier to increase peak-negative pressure with focused beams. However, it would remove one of the advantages of plane wave imaging,

which is that tissue is insonified uniformly and that evolution is observed simultaneously over the whole plane.

For the microbubbles to be activated and show postdisruption peak enhancement, pulses have to be longer than 100 μs. As the disruption pulse gets longer, the peak enhancement is increased until attaining a maximum at 500 μs. It is interesting to note that a slight disruption of the microbubbles was induced by the imaging pulses themselves, as shown by their linear decay for the short pulses.

An important element in 2D dissolution imaging is the dependence on position. As seen in Figure 2 and Figure 5, bubble signal at the top of the vessel collapsed much faster than the other microbubbles. This is consistent with the effect of acoustic pressure which pushes the microbubbles away from the transducer. A fraction of the increase in scattering of the centre of the vessel is probably due to the microbubbles displaced from the top. However, for a range of pulse pressures and lengths, postdisruption peak enhancement is present everywhere, showing that the effect is mainly intrinsic to the microbubbles. In Figure 5, peak enhancement is maximal at 2 mm from the top of the vessel. Deeper, peak enhancement is reduced and a lower proportion of microbubbles are ultimately destroyed at the end of dissolution. This is consistent with attenuation, which reduces the amplitude of the disruption signal at higher depth.

The spatial heterogeneity of microbubble dissolution can be exploited for contrast imaging. Figure 6f highlights the variation between microbubbles near a boundary and those in the centre of the vessel. Such dipole behaviour shows the effect of acoustic pressure on the microbubbles. Since imaging is done very rapidly, it would be minimally affected by arterial flow. Such geometric dependence could be exploited to assess the efficacy of microbubble targeting aided by acoustic pressure (Dayton et al. 1999).

The other images in Figure 6 show the results of more classic pulse sequences but performed with plane waves. Ultrafast allows addition (PWPI) or subtraction (PWAM) of entire images taken with little time difference. Such frame rates can reduce the effect of motion or avoid speckle variations between lines. Amplitude modulation, a three-pulse method, seems to provide a better CTR than pulse-inversion, a two-pulse method. Since ultrafast beamforming is performed by software, the displayed frame rate is dependent on the processor speed.

The dissolution of microbubbles is dependent on their position within the vessel. It has been shown to be affected by the surrounding hydrostatic pressure of its environment (Bouakaz et al. 1999). Bound microbubbles, such as those targeting diseased cells, should also be affected by their anisotropic medium. As shown by Figures 7 and 8, microbubbles bound to a gelatin surface dissolve much faster than those in solution. The fact that their membrane is attached to a surface might induce fragmentation more easily, yielding smaller bubbles. However, this observation needs to be confirmed with high-speed optical cameras. Independently of the process that causes such a contrast, the difference in dissolution between bound and free-flowing agents could become very relevant for ultrasound molecular imaging. Currently, free-flowing microbubbles have to be cleared from the imaging plane before molecularly-specific microbubbles are imaged, which takes several minutes (Christiansen and Lindner 2005). Dissolution imaging of the microbubbles might alleviate such a need for clearance.

The development of ultrafast imaging allows the transfer of laboratory knowledge to *in vivo* imaging. For instance, high frame-rate monitoring of drug delivery with gaseous or vaporizable agents might give additional information on its effectiveness. Doppler imaging of microbubbles could also be performed with a much higher temporal resolution. Finally, noninvasive assessment of the hydrostatic pressure might be possible over a whole imaging plane.

CONCLUSION

This study demonstrated that ultrafast ultrasonic imaging can provide new insights on the dynamic of microbubbles. Transient phenomena such as microbubble dissolution are invisible to conventional ultrasound scanners but were exposed by plane-waves emitted at a kHz rate. This method highlighted the peak in backscattering intensity following the disruption pulse. Such enhancement can increase the contrast from microbubbles in disruption-reperfusion imaging. Moreover, tracking the dissolution helped distinguish microbubbles near a wall or bound to a surface from the free-flowing agents. Such high temporal resolution could lead to new contrast imaging modalities in order to highlight, for example, the attachment of microbubbles to diseased cells or changes in hydrostatic pressure.

Acknowledgements—The authors thank Dr. M. Arditi and Bracco Research (Switzerland) for providing the contrast agents. This work was supported by the Fondation Pierre-Gilles de Gennes.

REFERENCES

Bercoff J, Tanter M, Fink M. Supersonic shear imaging: A new technique for soft tissue elasticity mapping. IEEE Trans Ultrason Ferroelectr Freq Control 2004;51:396–409.

Bercoff J, Tanter M, Chaffai S, Fink M. Ultrafast imaging of beamformed shear waves induced by the acoustic radiation force. Application to transient elastography. IEEE Ultrason Symp 2002. Q10

Bevan PD, Karshafian R, Burns PN. The influence of fragmentation on the acoustic response from shrinking bubbles. Ultrasound Med Biol 2008;34:1152–1162.

Bevan PD, Kashaffian R, Tickner EG, Burns PN. Quantitative measurement of ultrasound disruption of polymer-shelled microbubbles. Ultrasound Med Biol 2007;33:1777–1786.

Bouakaz A, Frinking PJA, de Jong N, Bom N. Noninvasive measurement of the hydrostatic pressure in a fluid-filled cavity based on the disappearance time of micrometer-sized free gas bubbles. Ultrasound Med Biol 1999;25:1407–1415.

Bouakaz A, Jong ND. WFUMB safety symposium on echo-contrast agents: Nature and types of ultrasound contrast agents. Ultrasound Med Biol 2007;33. 197–196.

Bouakaz A, Versluis M, Jong ND. High-speed optical observations of contrast agent destruction. Ultrasound Med Biol 2005;31:391–399.

Caskey CF, Stieger SM, Qin S, Dayton PA, Ferrara KW. Direct observations of ultrasound microbubble contrast agent interaction with the microvessel wall. J Acoust Soc Am 2007;122:1191–1200.

Chen WS, Matula TJ, Crum LA. The disappearance of ultrasound contrast bubbles: Observations of bubble dissolution and cavitation nucleation. Ultrasound Med Biol 2002;28:793–803.

Chomas JE, Dayton P, May D, Ferrara K. Threshold of fragmentation for ultrasonic contrast agents. J Biomed Opt 2001;6:141–150.

Christiansen JP, Lindner JR. Molecular and cellular imaging with targeted contrast ultrasound. Proc IEEE 2005;43:809–818.

Couture O, Sprague M, Cherin E, Burns PN, Foster FS. Reflection from bound microbubbles at high ultrasound frequencies. IEEE Trans Ultrason Ferroelectr Freq Control 2009;56:536–545.

Dayton P, Klibanov A, Brandenburger G, Ferrara K. Acoustic radiation force *in vivo*: A mechanism to assist targeting of microbubbles. Ultrasound Med Biol 1999;25:1195–1201.

Dayton P, Rychak J. Molecular ultrasound imaging using microbubble contrast agents. Frontiers Biosci 2007;12:5124–5142.

Deffieux T, Gennison JL, Tanter M, Fink M, Nordez A. Ultrafast imaging of *in vivo* muscle contraction using ultrasound. Applied Phys Lett 2006;89:184107.

Eckersley RJ, Chin CT, Burns PN. Optimising phase and amplitude modulation schemes for imaging microbubble contrast agents at low acoustic power. Ultrasound Med Biol 2005;31:213–219.

Garbin V, Cojoc D, Ferrari E, Di Fabrizio E, Overvelde MLJ, van der Meer SM, de Jong N, Lohse D, Versluis M. Changes in microbubble dynamics near a boundary revealed by combined optical micromanipulation and high-speed imaging. Appl Phys Lett 2007;90:114103.

de Jong ND, Frinking PJA, Bouakaz A, Ten Cate FJ. Detection procedures of ultrasound contrast agents. Ultrasonics 2000;38:87–92.

de Jong ND, Emmer M, Chin C, Bouakaz A, Mastik F, Lohse D, Versluis M. "Compression-only" behavior of phospholipid-coated contrast bubbles. Ultrasound Med Biol 2007;33:653–656.

Masoy S, Standal O, Nasholm P, Johansen TF. SURF imaging: *In vivo* demonstration of an ultrasound contrast agent detection technique. IEEE Trans Ultrason Ferroelectr Freq Control 2008;55:1112–1121. Q11

Montaldo G, Tanter M, Bercoff J, Benech N, Fink M. Coherent plane wave compoundingfor very high frame rate ultrasonography transient elastography. 2008;56:489–506. Q12

Muller M, Gennisson JL, Deffieux T, Tanter M, Fink M. Quantitative viscoelasticity mapping of human liver using supersonic shear imaging: Preliminary *in vivo* feasibility study. Ultrasound Med Biol 2008. Q13

Porter TR, Xie F. Transient myocardial contrast after initial exposure to diagnostic ultrasound pressures with minute doses of intravenously injected microbubbles demonstration and potential mechanisms. Circulation 1995;92:2391–2395.

Postema M, Bouakaz A, Versluis M, de Jong N. Ultrasound-induced gas release from contrast agent microbubbles. Ultrasonics 2005;52:1035–1041. Q14

Postema M, Jong ND, Schmitz G. Shell rupture threshold, fragmentation threshold, blake threshold. IEEE Ultrason Symp 2005. Q15

Sandrin L, Tanter M, Catheline S, Fink M. Shear modulus imaging with 2-D transient elastography. IEEE Trans Ultrason Ferroelectr Freq Control 2002;49:426–435. Q16

Sarvazyan AP, Rudenko OV, Swanson SD, Fowlkes JB, Emelianov SY. Shear wave elasticity imaging: A new ultrasonic technology of medical diagnostics. Ultrasound Med Biol 1998;24:1419–1436.

Shattuck DP, Weinshenker MD, Smith SW, von Ramm OT. Explososcan: A parallel processing technique with high speed ultrasound imaging with linear phased arrays. J Acoust Soc Am 1984;75:1273–1282.

Simpson DH, Chin CT, Burns PN. Pulse inversion Doppler: A new method for detecting nonlinear echoes from microbubble contrast agents. IEEE Trans Ultrason Ferroelectr Freq Control 1999;46:372–382.

Tanter M, Bercoff J, Athanasiou A, Deffieux T, Gennisson JL, Montaldo G, Muller M, Tardivon A, Fink M. Quantitative assessment of breast lesion viscoelasticity: Initial clinical results using supersonic shear imaging. Ultrasound Med Biol 2008;34:1373–1386.

Tanter M, Bercoff J, Sandrin L, Fink M. Ultrafast compound imaging for 2-D motion vector estimation: Application to transient elastography. IEEE Trans Ultrason Ferroelectr Freq Control 2002;49:1363–1374.

Wei K, Jayaweera AR, Firoozan S, Linka A, Skyba DM, Kaul S. Quantification of myocardial blood flow with ultrasound-induced destruction of microbubbles administered as a constant venous infusion. Circulation 1998;97:473–483.

Wilson SR, Burns PN. Microbubble contrast for radiological imaging: 2. Applications. Ultrasound Q 2006;22:5–13.

Zhao S, Ferrara K, Dayton P. Asymmetric oscillation of adherent targeted ultrasound contrast agents. Appl Phys Lett 2005;87:8459.